

The lowermost mantle beneath northern Asia—II. Evidence for lower-mantle anisotropy

Ch. Thomas^{1,*} and J.-M. Kendall²

¹Department of Earth Sciences, University of Liverpool, Liverpool, L69 3GP, UK. E-mail: tine@liv.ac.uk

²Department of Earth Sciences, University of Leeds, Leeds, LS2 9JT, UK

Accepted 2002 May 8. Received 2002 April 26; in original form 2000 May 12

SUMMARY

We have analysed prediffracted *S*-waves with turning points beneath northern Siberia in a study of anisotropy in the lowermost mantle. Deep-focus earthquakes beneath the Marianas, Izu Bonin and the Sea of Japan recorded at stations in western Europe are used. A correction for upper-mantle anisotropy is applied to the data. Comparisons of the data with synthetic data for models with and without a high velocity *D*' layer suggest that there is a velocity discontinuity at the top of the *D*' region and that the style of anisotropy is transversely isotropic in this region. Time separations between *S*-waves on the radial and transverse component show a weak trend where the separation increases with epicentral distance. A normalization of this separation with the travel distance within *D*' (300 km thick in this region) suggests that the anisotropy is uniformly distributed within this layer and has an average value of 0.5 per cent. A combination of different studies which investigate the structure of the lowermost mantle beneath Europe and northern Siberia reveals a complicated picture. Tomographic models from this area and evidence of *D*' anisotropy, lower mantle scatterers, reflections from a *D*' discontinuity and ultra-low-velocity zones suggest two distinct regions. One exhibits high velocities, *D*' anisotropy, a *D*' discontinuity and no evidence of scatterers or ultra-low-velocity zones. These features are likely associated with the palaeosubduction of the Izanagi plate well into the lowermost mantle. The other region has a lower overall velocity and shows evidence of scatterers and ultra-low-velocity zones, perhaps suggesting the presence of partial melt. These results suggest dramatic lateral variations in the nature of the lowermost mantle beneath northern Asia over a length scale of roughly 30 degrees.

Key words: anisotropy, *D*', lower mantle, *S*-wave, seismology.

1 INTRODUCTION

As the number of studies of the structure of the lower mantle increases, the emerging picture of the *D*' region (lowermost 200–400 km of mantle) is one of considerable complexity. A geographical region which has been studied extensively is that beneath northern Europe and Asia. Here the *D*' region exhibits heterogeneity on many length scales. In this paper we investigate seismic anisotropy in this area for the first time.

Tomographic models (Grand *et al.* 1997; Karason & van der Hilst 2000; Ritsema *et al.* 1999) show a fast region in the lowermost mantle beneath northern Siberia which may be associated with the downgoing remnants of the Izanagi slab which subducted ~80 Ma (Lithgow-Bertelloni & Richards 1998). Further to the east, the region beneath northern Europe exhibits average to slightly slow velocities in these tomographic models.

Some of the earliest evidence for a *D*' discontinuity has come from this region (e.g. Lay & Helmberger 1983, found evidence for a *S*-wave discontinuity). Since then there has been considerable evidence for an abrupt increase in *P*- and *S*-wave velocities which shows significant large-scale and short-scale variations in location and impedance contrast (e.g. Weber & Davis 1990; Gaherty & Lay 1992; Weber 1993; Houard & Nataf 1993; Kendall & Shearer 1994; Thomas & Weber 1997). The data used for these studies were mainly events from the region Japan/Kurile Islands recorded in Europe. In the first paper of this series (Thomas *et al.* 2002) we confirmed the existence of the discontinuity using Hindu Kush events recorded at stations of the Canadian National Seismograph Network (CNSN), source–receiver paths which are roughly orthogonal to the northwest Pacific to Europe paths.

In recent years Garnero and colleagues have found evidence for patches of ultra-low velocity zones at the core–mantle boundary (CMB). Garnero & Helmberger (1995, 1998) found evidence for ultra-low-velocity zones beneath Scandinavia and no evidence for ultra-low-velocity zones beneath Siberia and central to southern

*Previously at: Department of Earth Sciences, University of Leeds, UK.

Europe. Evidence for heterogeneity on a smaller scale comes from studies of lower-mantle scatterers. Using earthquakes from the New Hebrides recorded in Germany, Thomas *et al.* (1999) found lower mantle scatterers beneath northern Europe. Vidale & Hedlin (1998) and Wen & Helmberger (1998) found scatterers in the lower mantle using Tonga Fiji events recorded in Norway. The scattering region in their study is slightly northeast of the region found by Thomas *et al.* (1999).

In this study we use deep-focus earthquakes from the northwest Pacific rim recorded at European stations to establish the nature

of anisotropy in the region beneath northern Siberia. The mechanisms which give rise to anisotropy (e.g. the preferred orientation of crystals or inclusions) are associated with deformation. In this way, evidence of anisotropy may tell us more about the dynamics of this region than does evidence of heterogeneity. Studies of anisotropy in the lowermost mantle (Vinnik *et al.* 1989, 1995; Kendall & Silver 1996, 1998; Matzel *et al.* 1996; Garnero & Lay 1997; Lay *et al.* 1989) have shown that anisotropy exists within D', but the coverage is far from global. The style of anisotropy seems to vary between regions with many appearing to be transversely isotropic

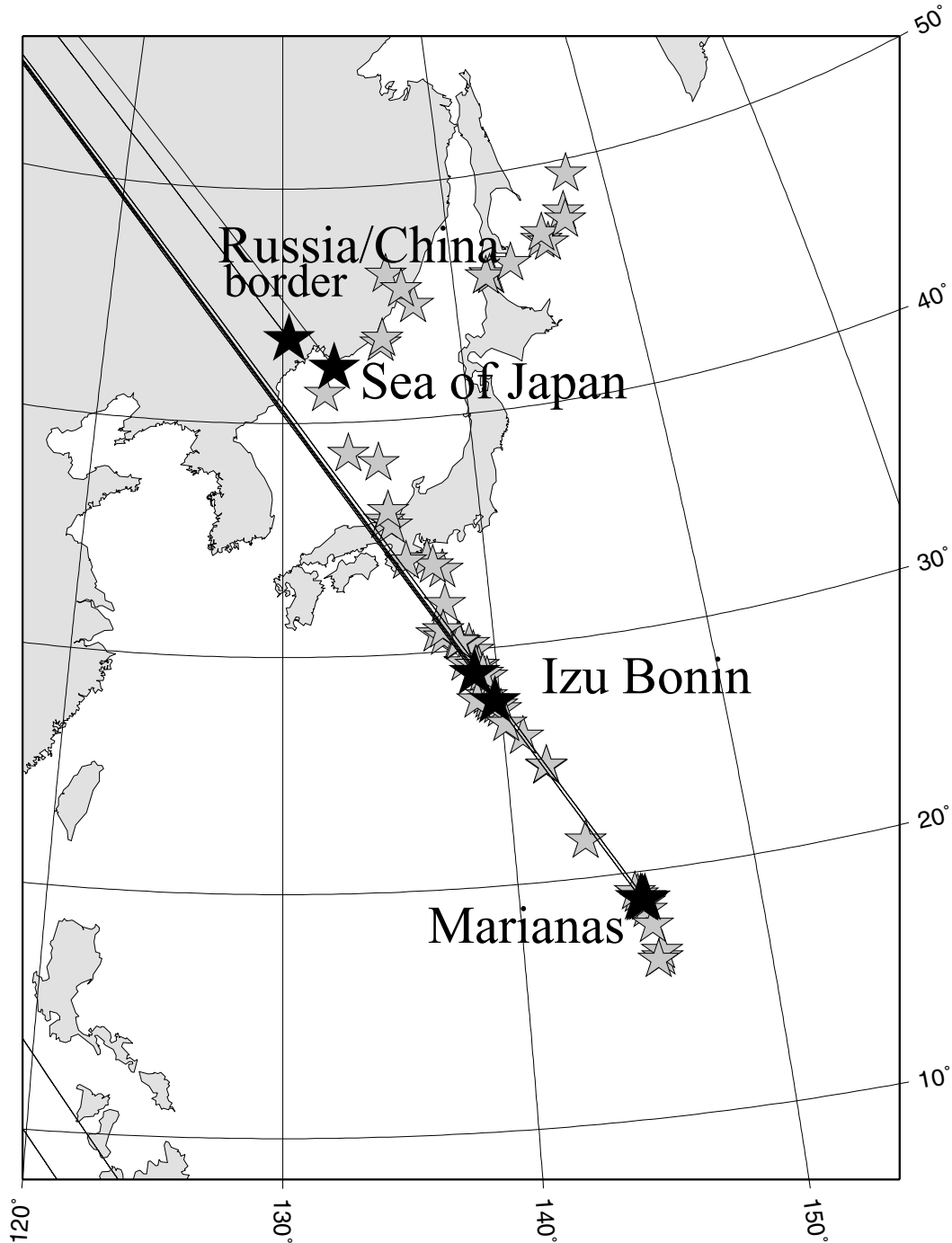


Figure 1. Epicentres of deep events in the North Pacific with a depth greater than 450 km. Black stars show events that have been used in the analysis, grey stars show epicentres where the signal-to-noise is not good enough or the focal mechanisms was such that the S-wave on either the transverse or on the radial component were weak. The black lines extending from the epicentres show the great circle paths to the station MOX.

Table 1. Earthquakes from the north Pacific used in this study. Earthquake Parameters are from the Harvard CMT catalogue. Backazimuth and distance are for the station MOX in Germany.

#	OT	Lat (deg N)	Lon (deg E)	Depth (km)	mb	Baz (deg)	Distance (deg)
1	20-Jan-92 13:37:03.08	27.98	139.40	498	6.0	44.4	89.1
2	21-Jul-94 18:36:31.74	42.34	132.87	471	7.3	41.2	74.2
3	23-Aug-95 07:96:02.76	18.86	145.22	594	7.1	44.1	99.7
4	24-Aug-95 01:55:34.63	18.90	145.05	587	6.2	44.2	99.6
5	24-AUG-95 06:28:54.92	18.85	145.12	602	5.8	44.2	99.6
6	16-Mar-96 22:04:06.24	28.98	138.94	477	6.7	44.2	88.1
7	26-Jun-96 03:22:03.14	27.73	139.75	468	6.3	44.2	89.5
8	08-Apr-99 13:10:34.08	43.61	130.35	565	7.1	42.0	72.1

(e.g. Caribbean, Kendall & Silver 1996, 1998, northern Pacific Garnero & Lay (1997); Matzel *et al.* (1996)); and others appearing more general in symmetry (Pulliam & Sen 1998; Russell *et al.* 1999). Maupin (1994) has shown that some effects interpreted as anisotropy

can be explained by isotropic models in the case of diffracted *S*-waves. We therefore compare synthetic data produced for isotropic models with and without a *D'* discontinuity to our data in order to guide our interpretation of anisotropy. We are also careful to correct for the effects of anisotropy in the upper-mantle beneath the receiver.

2 DATA

We have analysed deep events in the Russia/China border region, Sea of Japan, Izu Bonin and the Marianas. These events lie along similar great circle paths to stations in Europe thereby enabling a study of variations in lower-mantle anisotropy for different epicentral distances and bottoming depths beneath northern Asia. To mitigate the effects of near-source anisotropy we restrict our analyses to events with depths greater than 450 km (below the olivine stability field). The grey stars in Fig. 1 show epicentres of events that could not be used due to poor signal-to-noise ratios or poor *S*-wave radiation. The black stars show epicentres of the 8 events that have been used for

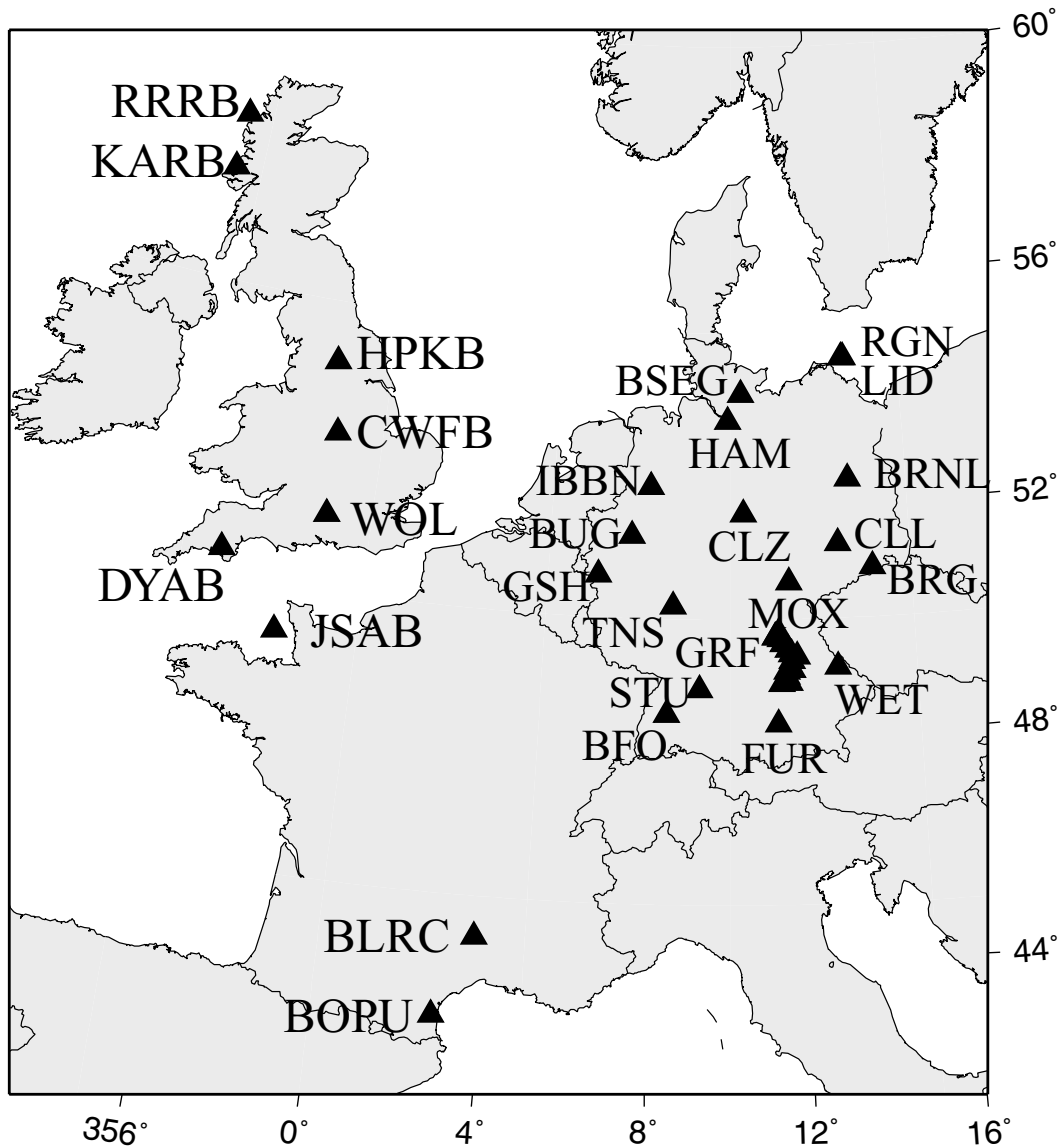


Figure 2. The stations of the German Regional Seismic Network (GRSN) and the SPICED array which extends across the UK and France. The station WOL is operated by the MOD, Blacknest, UK.

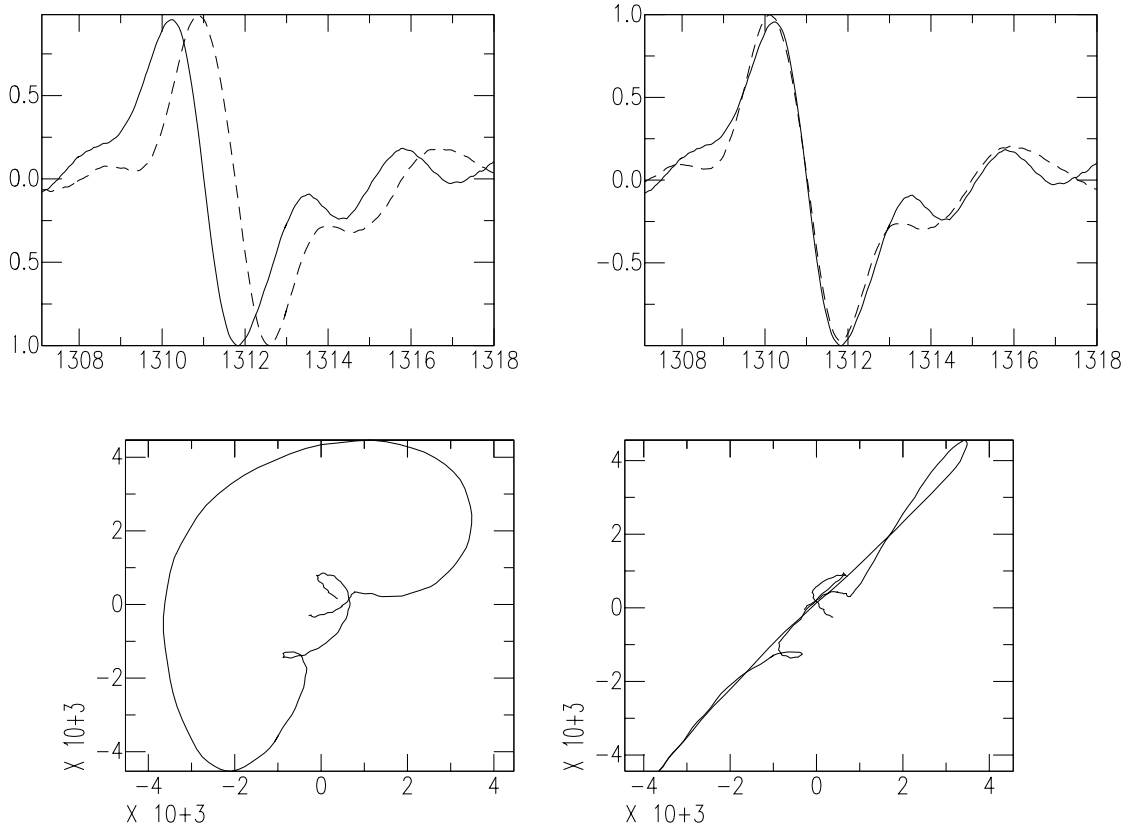
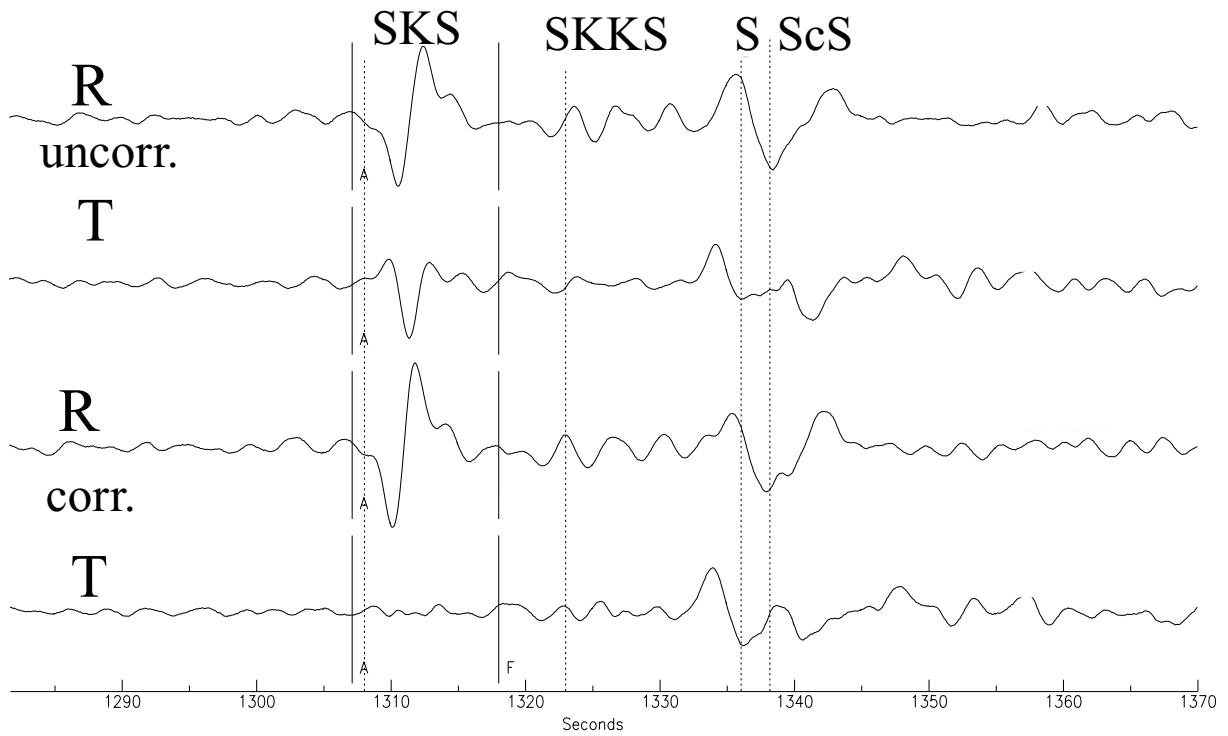


Figure 3. Upper-mantle anisotropy correction for one station (GRA1) and an event in the Izu Bonin region (event 1). The top two traces show the uncorrected case. *SKS* is visible on the transverse component. After applying the correction the *SKS* arrival is not visible on the transverse component and a clear separation between the *S*-wave on the transverse and radial component is visible (bottom two traces). The bottom of the figure shows the slow and fast shear waves and the particle motion before and after the correction.

this study (Table 1). The black lines emerging from the epicentres indicate the great circle path to the station MOX in Germany. The stations used in this study are shown in Fig. 2. The data are bandpass filtered (3–50 s) records of ground velocity.

Before looking for anisotropy in the lowermost mantle, we have to first correct the data for the effects of upper-mantle anisotropy. An example of this correction is shown in Fig. 3. The degree of *SKS*-splitting and the polarizations of the fast and slow shear waves are measured using the methodology of Silver & Chan (1991). The corrected traces show no *SKS* energy on the transverse component

but there is still a clear separation between the *S*-waves on both components. The events that did not show a clear *SKS* signal have been corrected using values for the stations given by Brechner *et al.* (1998).

For events beyond 88° in epicentral distance, the *S* and *ScS* merge making it difficult to distinguish one from the other, but these phases have long paths through the D'' region. We avoid phases diffracted considerable distances along the CMB ($>103^\circ$) to minimize core coupling effects (Maupin 1994). After application of the upper-mantle correction we find that most source–receiver pairs show a

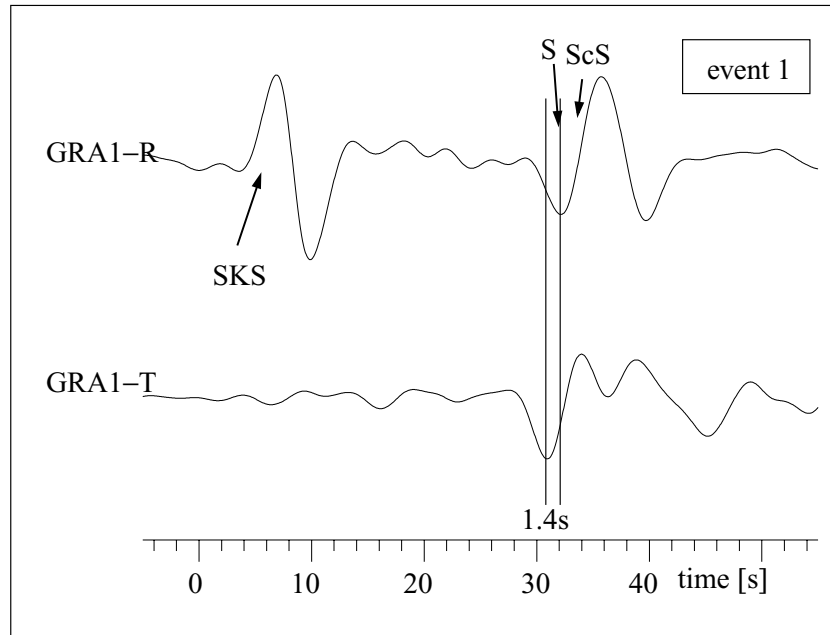


Figure 4. Upper-mantle anisotropy–corrected radial (R) and transverse (T) components for event 1 from Table 1 recorded at GRA1. The epicentral distance for this event is 90.0° . The minimum of the *S*-wave is marked in both traces with the black bar. A time separation between the minimum of the *S*-wave on the R and T component of 1.4 s is visible with the transverse leading the radial component.

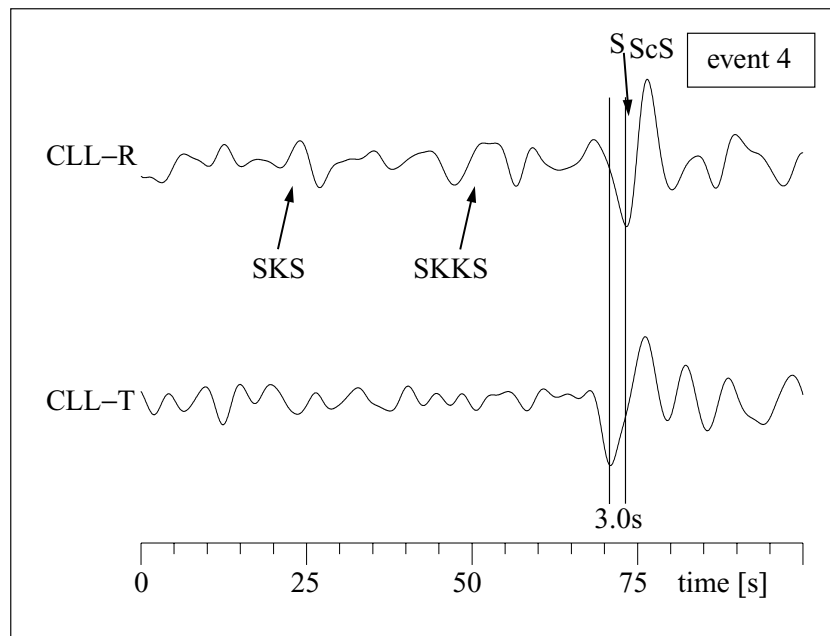


Figure 5. As Fig. 4 but for a Mariana event (event 4 from Table 1) recorded at CLL. The epicentral distance is 98.5° and the time separation is 3.0 s.

clear time separation between the *S-ScS* phase on the radial and transverse component. Figs 4 and 5 show two examples. In both cases the *S*-wave in the transverse component is leading the *S*-wave on the radial component, as is the case for >95 per cent of the data. The epicentral distance for the station GRA1 and the event from the Izu Bonin region in Fig. 4 is 90.0°. The turning point of the

S-wave is at a depth of 2646 km (i.e. the wave samples the upper part of the *D''* region). The separation between radial and transverse components is 1.4 s. Fig. 5 is a recording at the station CLL of an event in the Marianas. The epicentral distance is 98.5° and the bottoming depth of the *S*-wave is 2773 km. The time lag between the radial and transverse component is 3 s.

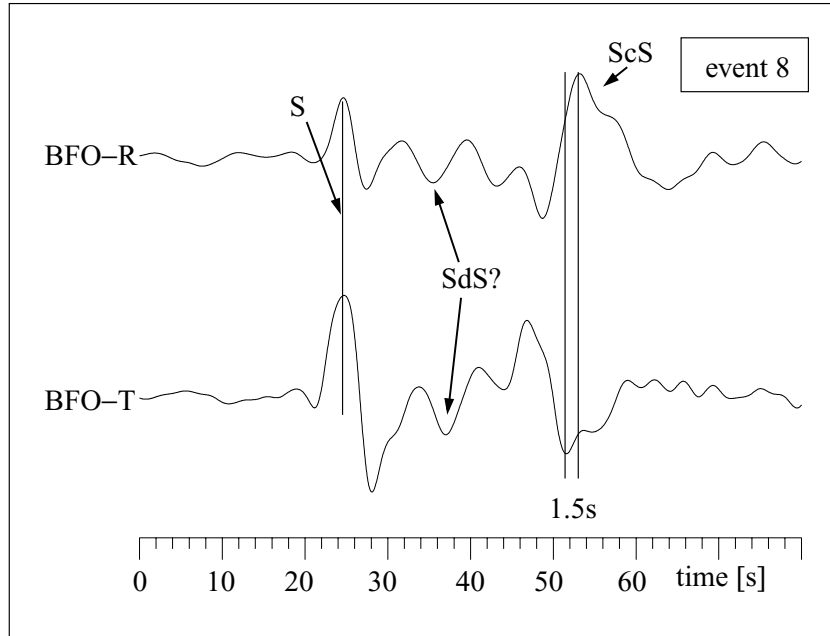


Figure 6. Upper-mantle anisotropy-corrected R and T component for the BFO recording of the event at the Russia/China border region. The epicentral distance for this source–receiver combination is 75.2°. The *S*-wave is marked. A time separation between *ScS* on the transverse and radial component of 1.1 s is visible. Also *SdS*, the reflection from the top of the *D''* discontinuity appears in the *S* coda.

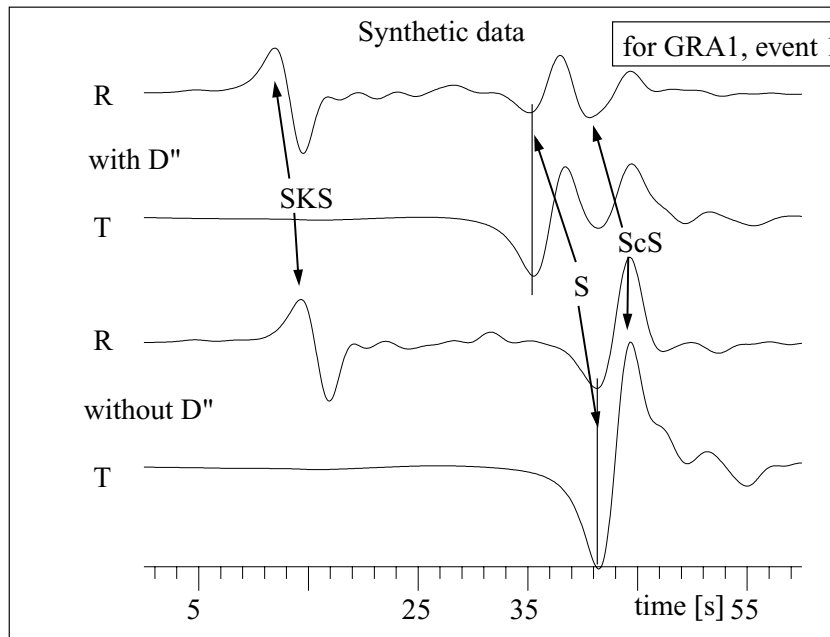


Figure 7. Synthetic data for event 1 from Table 1 for station GRA1 (compare with Fig. 4). The top two traces are radial (R) and transverse (T) components for a model with a velocity increase of 3 per cent at a depth of 2065 km. The bottom two traces are R and T component for the model ak135 without *D''* discontinuity. The minima of the *S*-wavelets are indicated by the vertical lines. No time separation between the *S*-waves on the transverse and radial component is visible. The *S*-wave for a model with a velocity discontinuity in the lowermost mantle arrives earlier compared to the model without *D''* discontinuity. This is due to the faster velocities within the *D''* layer. The synthetic data show that we can measure time separation by picking the first minimum of the *S*-waves.

For the nearer events (Sea of Japan and Russia/China border region) we measure the differential traveltime between S and ScS on the radial and transverse component again after a correction for upper-mantle anisotropy. The distance range for these events is between 68.5 and 81.9° for the stations we used. At these distances the S -wave turns above the D'' region and therefore will not be influenced by anisotropy within D'' . Fig. 6 shows an example for one source–receiver combination (Russia/China border region event recorded at BFO). The difference between residual travel times (S - ScS (transverse) and S - ScS (radial)) is 1.1 s. Also visible in the data is

the reflection from the top of the D'' discontinuity (SdS) and the diving wave into D'' (SDS) which at this distance arrives approximately between S and ScS .

3 SYNTHETICS

If the style of D'' anisotropy is transverse isotropy, that is hexagonal symmetry with a vertical symmetry axis, the radial and transverse components will record the fast and slow shear-waves independently. Furthermore, the waveforms will look like those for the

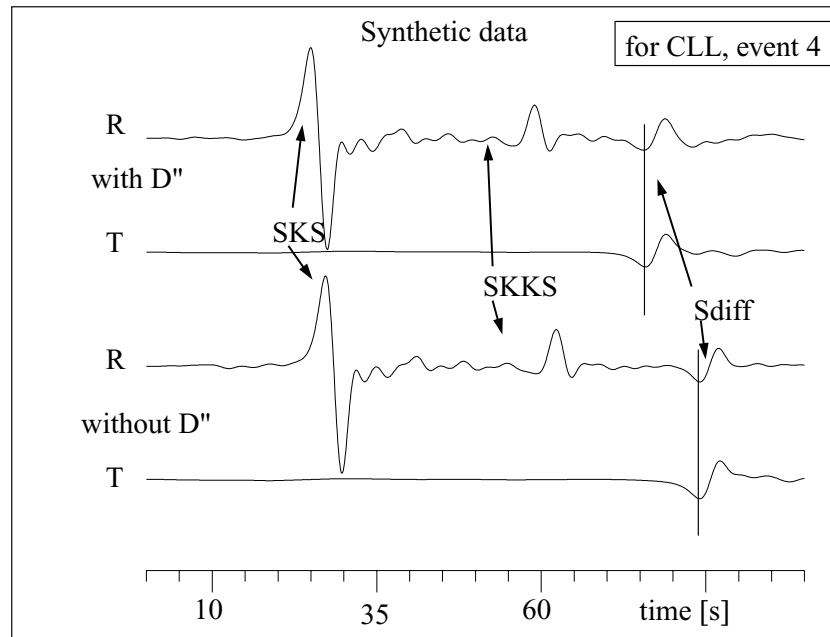


Figure 8. As for Fig. 7 but for event 4 and station CLL (compare with Fig. 5). The top two traces are radial and transverse components for the model with a D'' discontinuity, the bottom two traces for a model without a D'' discontinuity (ak135).

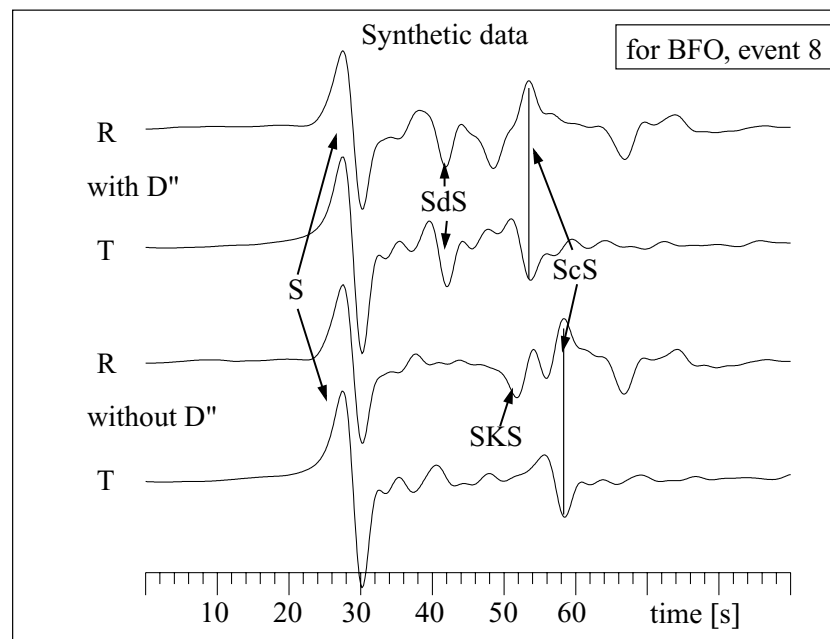


Figure 9. As for Fig. 7 but for event 8 and station BFO (compare with Fig. 6). SdS refers to the reflection from the D'' discontinuity. For the model with the higher velocity in D'' the ScS -wavelet merges with the SKS -wavelet (top two traces).

isotropic case, but there will be a simple time shift between the components. If the anisotropy is more general, either due to an inclined symmetry axis or a system with less symmetry than the hexagonal case, the radial and transverse waveforms will contain a combination of the fast and slow shear-waves. The waveforms will not look like those in the isotropic case. To assess this in the data we generate synthetic seismograms for isotropic models with and without a D'' discontinuity.

We use the reflectivity method (Müller 1985) and include the Harvard focal mechanism for each earthquake to calculate the synthetic data. The reference model is ak135 (Kennett *et al.* 1995) with a D'' model for this region superimposed. The region beneath northern Siberia shows a discontinuity above a high velocity D'' layer. A number of P - and S -wave models exist for this region but the discontinuity is roughly at a depth of 2605 km and shows an S -wave velocity increase ≤ 3 per cent (SWDK: 3 per cent, Weber & Davis 1990, SGL: 2.75 per cent, Gaherty & Lay (1992); SNSA: 2.3 per cent and SNSB: 2.6 per cent, Weber (1993)). We use SWDK and its P -wave equivalent PWDK to calculate the reflectivity synthetics and the resulting seismograms are filtered with the same bandpass filter (3–50 s) as the real data to aid comparison.

Fig. 7 shows synthetic data for the example given in Fig. 4 for a model with (top two traces) and without (bottom two traces) a discontinuity at the top of D'' . The results for each model are quite different and the data clearly do not match the waveforms for the model without a discontinuity. The waveform data and the waveforms for the SWDK model are very similar in shape but the data show a large time separation between the radial and transverse components which is not apparent in the synthetics. This is a strong indication that the style of anisotropy is most likely transversely isotropic. This also helps guide our picks of the relative separation between the radial and transverse components. For example, we can pick the first large maxima on each component which is much easier to pick than the onset of the S/ScS phase.

Fig. 8 shows the synthetic data for the example in Fig. 5. In this case there is less difference between the two sets of waveforms for each model. Here the epicentral distance is 98.5° . The S/ScS -Sdiff waveforms for each model become similar near the point of core

diffraction. The data still show a clear separation between components which is not visible in the synthetics. The relative amplitudes of the S - and SKS -waveforms are, although, quite different when comparing the data and synthetics. This may be due to inaccuracies in the estimated focal mechanism for this event.

The synthetic data for the event in Fig. 6 are shown in Fig. 9. In this case ScS arrives several seconds after S . The model with the D'' discontinuity produces an additional arrival (SdS , the reflection from the top of the discontinuity). Note that ScS for the model with a D'' discontinuity arrives early and merges with the SKS arrival. The synthetic data therefore suggest that it is best to pick the time of ScS after its initial onset at the first minimum or maximum depending on the component. Trying to pick the first onset of the ScS -wave would in this case give wrong results, thus illustrating the importance of using synthetics to guide the time picking for each event.

We have tried to cross-correlate the real data with the synthetic data in order to enhance the quality of our time picks. However, since the cross-correlation is very sensitive to the waveforms and we do not know the exact velocity structure in the lower mantle, the results from the cross-correlation can be misleading. To apply this technique, we need to know the exact velocity distribution within D'' to be able to compute waveforms which match the real data, especially because the SdS and SDS phases have a strong influence on the waveform. This is the reason why we can only use the synthetics data as a guideline to where to pick the time separation.

4 RESULTS

Using the synthetic data as a guideline we measure the time separation between the S -waves on the radial and transverse component. In over 95 per cent of the measurements, $S(ScS)$ on the transverse component is ahead of the arrival on the radial component. In general, the shape of the waveforms matched those predicted for the isotropic model with a D'' discontinuity thereby suggesting the style of anisotropy is transversely isotropic.

The time separations between the S -waves on the T and R component as a function of epicentral distance (Fig. 10a) shows some scatter but there is a weak trend suggesting larger separations as the

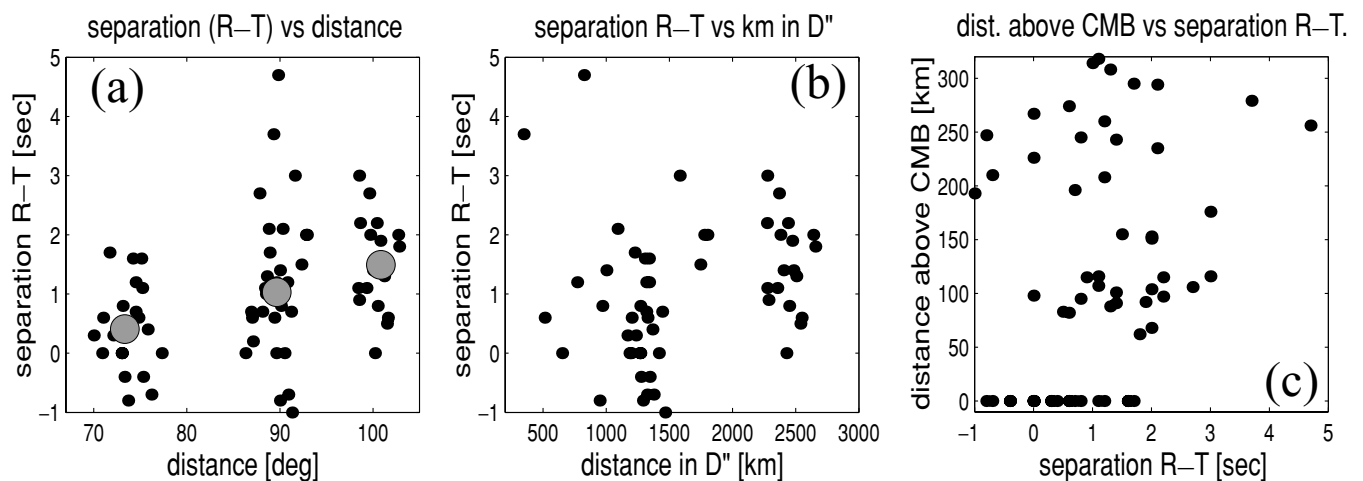


Figure 10. Results from the shear-wave splitting analysis for bandpass filtered data (50 to 3 s). (a) time separation of the S -wave on the transverse and radial component as function of epicentral distance. Negative measurements give cases, where the signal on the radial is leading the signal on the transverse component. Grey circles show mean values for each cluster (corresponds to regions in which events occur). The values are 0.42 for the closest cluster, 1.11 for the middle cluster and 1.49 for the cluster furthest away. The error in picking the separation times is ± 0.2 s. (b) Separation (R-T) as a function of travel distance within D'' . A 293 km thick D'' layer is assumed. (c) bottoming depth given as distance above the CMB as a function of time separation (R-T). The points at the CMB are bottoming points for the nearest cluster (Russia/China border and Sea of Japan) are at the CMB since we analyse ScS instead of S for these events.

epicentral distance increases. Averages for each cluster of points which correspond to the different epicentral regions (Japan, Izu Bonin, Marianas) are shown. Shear-wave splitting as a function of distance travelled within the D'' region (bottom 300 km) (Fig. 10b) again suggests an increase with distance with much scatter between measurements. Finally, there is no obvious correlation between splitting and the bottoming depth of the rays, here given as distance above the CMB (Fig. 10c) indicating that the anisotropy is uniformly distributed throughout the D'' region.

In order to assess the magnitude of the anisotropy we normalize the amount of splitting by the distance travelled in the D'' layer using

$$\delta t = t_{\text{slow}} - t_{\text{fast}} = \frac{d}{v - \frac{1}{2}av} - \frac{d}{v + \frac{1}{2}av} \quad (1)$$

which leads to

$$a = \frac{-2d}{v\delta t} \pm \sqrt{4 + \left(\frac{2d}{v\delta t}\right)^2}, \quad (2)$$

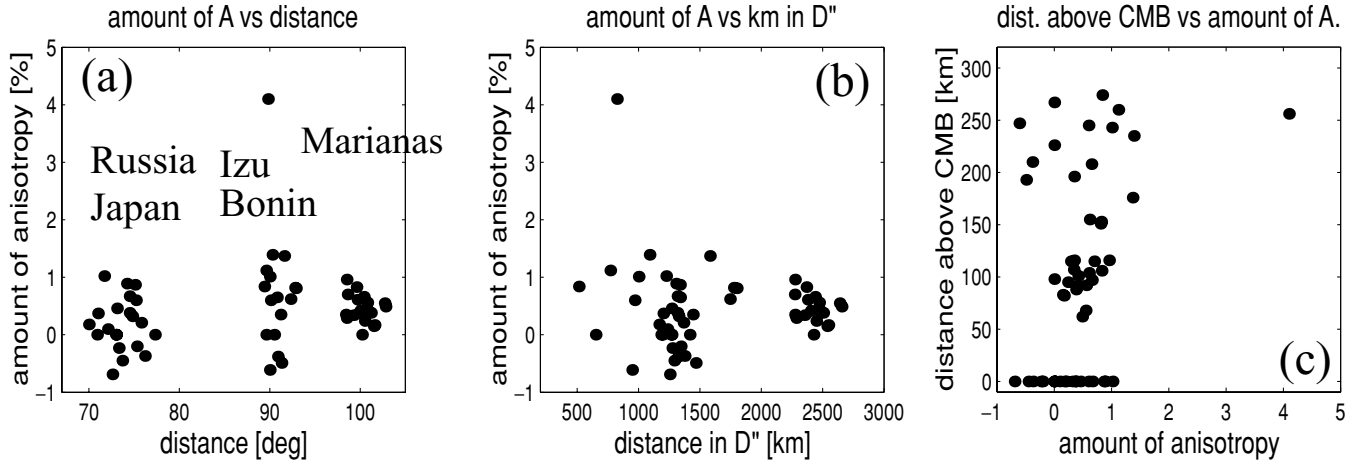


Figure 11. As for Fig. 10 but normalized with respect to the travel distance within D'' which gives the amount of anisotropy instead of the separation (R-T). The regions to which the data clusters correspond are also given.

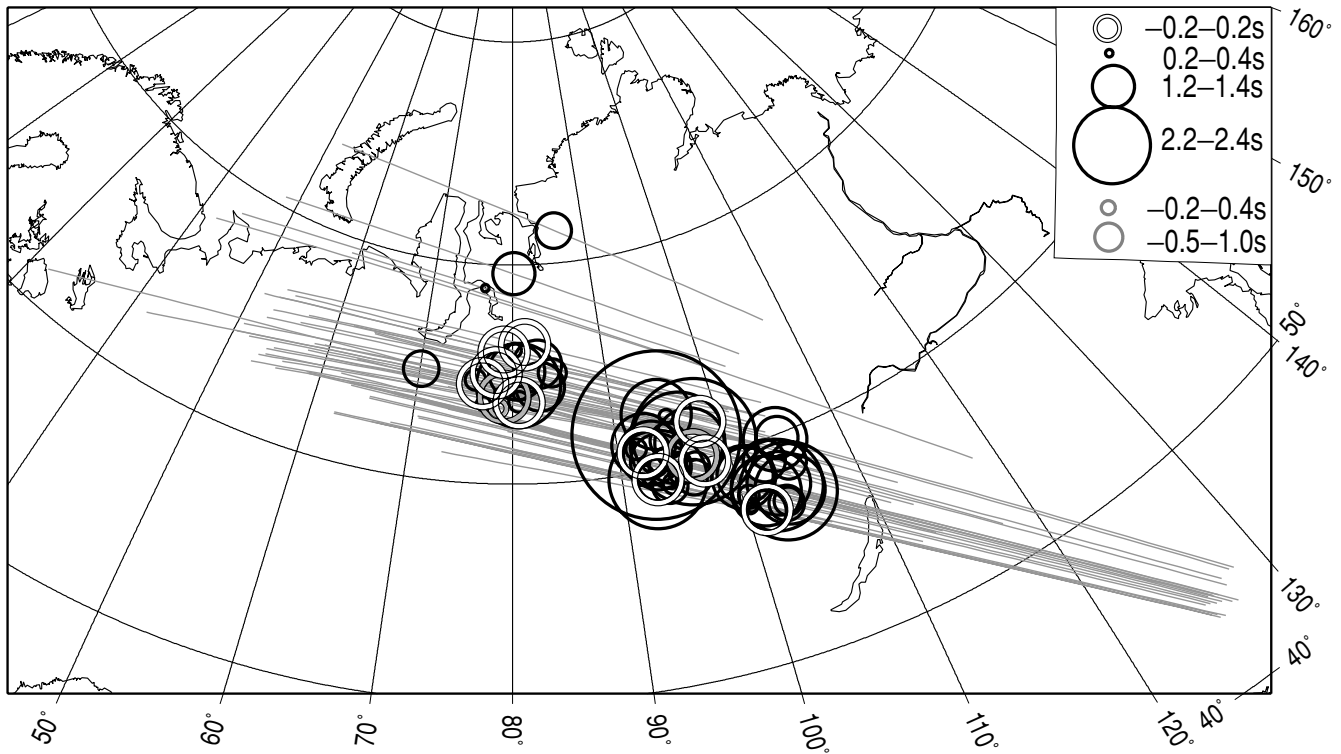


Figure 12. Travel paths (grey lines) within D'' of the analysed S (ScS)-waves. Based on the model SWDK (Weber & Davis 1990) entry into D'' is at 2605 km depth. The size of the circles at the midpoints of the lines show the time separation measurements. Black circles are cases where the signal on the transverse component is leading that on the radial component. Grey circles show the cases where the signal on the radial is leading that on the transverse component and white circles show cases, where the measurements agree with the accuracy of the measurements (± 0.2 s).

Table 2. Measured splitting parameters for *SKS* splitting. Numbers of events correspond to numbers in Table 1.

Station	Event	Baz	Φ	δt
BFO	1	42	69 ± 9	0.8 ± 0.2
BFO	3	42	59 ± 11	1.6 ± 0.5
BFO	5	42	72 ± 12	2.3 ± 0.5
BFO	6	42	74 ± 22.5	0.7 ± 1.1
BRG	3	46	-75 ± 10	0.8 ± 0.1
BRG	5	46	-74 ± 8	0.8 ± 0.1
BRG	6	46	-64 ± 22.5	0.7 ± 0.2
BRNL	1	46	-63 ± 7	0.7 ± 0.2
BRNL	6	46	-58 ± 2	1.9 ± 0.1
BSEG	6	43	-52 ± 22.5	0.7 ± 1.5
BUG	3	41	-64 ± 22.5	1.0 ± 2.5
BUG	6	41	-61 ± 18	0.8 ± 0.3
CLL	3	45	43 ± 4	1.5 ± 1.6
CLL	6	45	-66 ± 16	0.5 ± 0.3
CLZ	1	43	28 ± 11	1.1 ± 0.5
CLZ	3	43	8 ± 18	0.6 ± 0.2
CLZ	6	43	26 ± 22.5	1.1 ± 0.8
FUR	3	44	63 ± 22.5	1.0 ± 1.0
FUR	6	44	-85 ± 5	1.2 ± 0.1
GRFO	1	44	-82 ± 6	0.8 ± 0.1
GRFO	5	44	66 ± 22.5	1.4 ± 1.8
GRFO	6	44	-75 ± 7	1.5 ± 0.1
GSH	6	40	41 ± 22.5	1.7 ± 1.5
MOX	3	44	75 ± 12.5	1.0 ± 0.3
MOX	5	44	-76 ± 22.5	1.7 ± 2.9
MOX	6	44	-50 ± 22.5	0.9 ± 2.5
STU	6	42	-86 ± 7.5	1.4 ± 1.2
TNS	1	42	-67 ± 11	1.0 ± 0.3
TNS	5	42	-49 ± 22.5	1.2 ± 2.6
TNS	6	42	44 ± 11	2.2 ± 0.5
WET	1	45	80 ± 5	1.5 ± 0.1
WET	3	45	-77 ± 22.5	1.5 ± 2.4
WET	5	45	87 ± 22.5	1.5 ± 2.7
WET	6	45	78 ± 22.5	1.2 ± 1.2

where a is the fractional amount of anisotropy, δt the time separation, d the travel distance in D'' , and v the average velocity in D'' . As before, Fig. 11 shows the per cent anisotropy as a function of epicentral distance, the amount of anisotropy as a function of distance travelled in D'' and the bottoming depth as a function of the amount of anisotropy. In all three diagrams no trend for the amount of anisotropy is visible which implies that the anisotropy is evenly distributed through D'' .

Fig. 12 shows surface projections of the travel paths of the S -waves within D'' (for the closer events it shows the travel paths for ScS since S turns above D''). The circles at the midpoints of each line show the degree of shear-wave splitting along each path. Black circles show measurements where the transverse component leads the radial component, grey circles show the few measurements where the radial leads the transverse, and white circles show cases where there is no discernible splitting (± 0.2 s). There is no obvious spatial clustering of circle size or colour.

Predictions of palaeosubduction place the Izanagi plate at the base of the mantle in this region (Lithgow-Bertelloni & Richards 1998). This would explain the high velocities and perhaps implies that the anisotropy is associated with subduction. A slab colliding with the CMB would experience a high amount of shear deformation. This could lead to dislocation glide in lower-mantle crystal assemblages (Karato 1998) or lead to layering or a preferred orientation in inclusions (Kendall & Silver 1998). It is perhaps easier to envision

transverse isotropy resulting from a layering mechanism, but given our lack of knowledge of lower-mantle mineralogy and dislocation mechanisms we cannot rule out crystal orientation as a cause.

5 COMPARISON WITH OTHER STUDIES

As discussed in the introduction, the region of the lowermost mantle beneath Siberia and northern Europe has been studied using many different techniques and data. The structure in this region seems to be very complex, showing a wide range of heterogeneity at most scales. There is evidence of a discontinuity at the top of D'' , ultra-low-velocity zones in some areas and not others and lower mantle scatterers. This study shows that this region is also anisotropic.

These results are summarized in Fig. 13. The underlying tomographic model is the S -wave model of Grand *et al.* (1997). Blue regions show faster than average velocities, red regions are slower than average and yellow regions are average velocities. It seems that there are two distinct regions. In one region the velocities are fast in tomography models and there is abundant evidence for a D'' discontinuity (Fig. 13c). In the first paper of this series we confirmed this D'' discontinuity from an orthogonal azimuth. We also find this region to be anisotropic. The travel paths within D'' , indicated by the red lines (Fig. 13b), are mostly confined to this fast velocity region. Garnero *et al.* (1998) find no evidence for ultra-low-velocity zones in this fast region (dark blue regions) (Fig. 13 top). Predictions of subducted lithosphere (Lithgow-Bertelloni & Richards 1998) show that the position of the Izanagi plate lies east of the high velocity region (white circles in the bottom right corner in Fig. 13b). We speculate that the slab may broaden or buckle on its way into the lowermost mantle and may influence the more westerly region.

The second region shows average to slightly slow velocities in P and S tomographic models. In this region Thomas *et al.* (1999) found evidence for scatterers, most likely in the lowermost mantle. The region where scatterers have been studied is indicated by the blue to yellow area, with the scatterers shown in red in the top left corner (Fig. 13b). Garnero *et al.* (1998) find evidence for ultra-low-velocity zones in the same region (pink region, Fig. 13a). Note, that the areas indicated for ultra-low-velocity zones are the size of CMB Fresnel zones and show the maximum spatial resolution of the analysed waves.

These two distinct regions in the lower mantle give rise to a few interpretations:

- (i) The anisotropy may be associated with the deformation of slab material which has descended to the core–mantle boundary.
- (ii) The reflections from the top of the D'' discontinuity in this area have been previously interpreted as a reflection from a remnant slab (Scherbaum *et al.* 1997). The small-scale topography of the discontinuity may result from buckling of this slab as it collides with the core–mantle boundary (Christensen & Hofmann 1994).
- (iii) The observation of scatterers and ultra-low-velocity zones in the same area may indicate that scatterers are partial melt at the base of the mantle rather than small-scale topography of subducted lithosphere.

It is important to consider that the observations are limited by the source–receiver combinations that can be used to study the lower mantle. There are, for example, very few data to extend the investigation of scatterers further to the east. Tonga–Fiji events recorded in Norway (e.g. Vidale & Hedlin 1998) yield the opportunity to study a region slightly northeast of the area shown here. On the other hand it

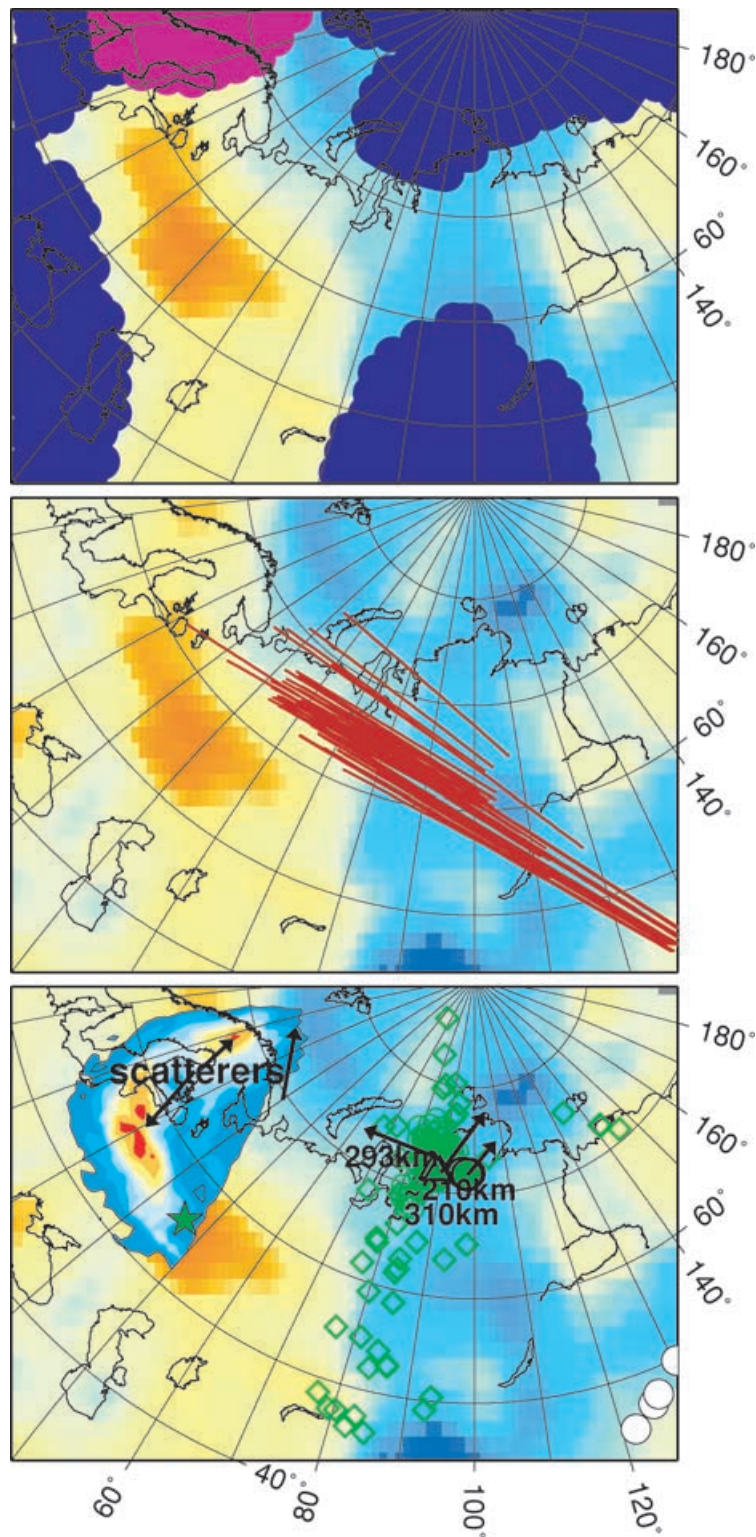


Figure 13. A presentation of results from a combination of different studies dealing with D' structure beneath northern Asia and Europe. The underlying tomographic image is from Grand *et al.* (1997). Bottom: Green symbols show reflection points from the top of the D' discontinuity. Open green circles are reflection points from North Pacific events (Kuriles) recorded in Germany (Thomas & Weber 1997). Filled green symbols are reflection points from Hindu Kush events recorded at stations in Canada (Thomas *et al.* 2002). The travel paths for these two studies are almost perpendicular at the crossing points. The thickness of the D' layer at the bounce points is also shown. Green open diamonds show reflection points from Gaherty & Lay (1992). The blue to yellow region in the top left corner shows the region where Thomas *et al.* (1999) searched for scatterers in the lower mantle and the red areas within these regions show the most likely location of scatterers (the result is for a layer 1 km above the core–mantle boundary). The white circles in the bottom right corner show the location of slabs in the lowermost mantle as predicted by Lithgow-Bertelloni & Richards (1998). Middle: The red lines indicate travel paths of S-waves (S_cS -waves) that have been used in this study to investigate anisotropy in the lowermost mantle. Top: Blue regions show regions where Garnero *et al.* (1998) found no evidence for ultra-low velocity zones, pink areas show regions where they found evidence for ULVZs. The regions indicate CMB Fresnel zones.

is difficult to extend the region where we find anisotropy into the average/slow region west of the studied region. Also, reflection points from the top of the D'' discontinuity are limited due to the sources and receivers currently available.

6 CONCLUSIONS

We have analysed S -waves from earthquakes beneath Russia, the Sea of Japan, Izu Bonin and the Marianas recorded at European stations. These events are roughly on the same great circle path but have epicentral distances from 68 to 102°. This allows us to study the radial distribution of anisotropy in the D'' region beneath Siberia. The region sampled by these data shows high velocities in tomographic models (e.g. Grand *et al.* 1997; Karason & van der Hilst 2000). After correcting for upper-mantle anisotropy, most source–receiver pairs show a time separation between the S -wave arrival on the transverse and radial component. In the case of the closer events (Russia and Sea of Japan, epicentral distance 68.5 to 80.4°) we measure the difference in residual traveltimes between the S - and ScS -waves on both components after correcting for upper-mantle anisotropy. 95 per cent of the data show the signal on the transverse component leading the signal on the radial component. The splitting values are up to 4.8 s with the average at 1.5 s. Waveform modelling of the data using an isotropic model shows similar waveforms compared to the data which suggests that the style of anisotropy is most likely transversely isotropic. The amount of anisotropy does not vary with the epicentral distance, the travel distance within D'' or with bottoming depth of the wave in D'' . This suggests that the anisotropy is distributed uniformly throughout the D'' region. The amount of anisotropy is found to be small, mean value ~ 0.5 per cent, with values up to ~ 1.3 per cent.

Combining studies of lower-mantle structure reveals two distinct regions in the lowermost mantle beneath Siberia and Northern Europe. Tomographic images show average to slightly slower than average velocities in one region where we also find small-scale structure associated with scatterers and ultra-low-velocity zones. In the other region which has higher than average velocities in tomographic models we find anisotropy as well as reflections from the discontinuity at the top of the D'' region and an absence of ultra-low-velocity zones.

Predictions of palaeosubduction place the Izanagi plate at the base of the mantle in this region (Lithgow-Bertelloni & Richards 1998). This would explain the high velocities and perhaps implies that the anisotropy is associated with the deformation of this plate as it collides with the CMB.

ACKNOWLEDGMENTS

We would like to thank Ed Garnero for his ultra-low-velocity zone locations, Jim Gaherty for his SdS bounce points, Carolina Lithgow-Bertelloni for plate locations and Steve Grand for his tomographic model. The data analysis was done using the program Seismic Handler by Klaus Stammler. All maps were produced using the program GMT by Wessel & Smith (1991). CT was supported by NERC grant GR3/12578 and DFG grant TH763/1–1.

REFERENCES

Brechner, S., Klinge, K., Krüger, F. & Plenefisch, T., 1998. Backscattered variations of Splitting parameters of teleseismic SKS phases observed at the broadband stations in Germany, *Pure appl. Geophys.*, **151**, 305–331.

- Christensen, U.R. & Hofmann, A.W., 1994. Segregation of subducted oceanic crust in the convecting mantle, *J. geophys. Res.*, **99**, 19 867–19 884.
- Gaherty, J.B. & Lay, T., 1992. Investigation of laterally heterogeneous shear velocity structure in D'' beneath Eurasia, *J. geophys. Res.*, **97**, 417–436.
- Garnero, E.J. & Helmberger, D.V., 1995. A very slow basal layer underlying large scale low-velocity anomalies in the lower mantle beneath the Pacific: Evidence from core phases, *Phys. Earth planet. Inter.*, **91**, 161–176.
- Garnero, E.J. & Helmberger, D.V., 1998. Further structural constraints and uncertainties of a thin laterally varying ultralow-velocity layer at the base of the mantle, *J. geophys. Res.*, **103**, 12 495–12 509.
- Garnero, E.J. & Lay, T., 1997. Lateral variations in lowermost mantle shear wave anisotropy beneath the north Pacific and Alaska, *J. geophys. Res.*, **102**, 8121–8135.
- Garnero, E.J., Revenaugh, J., Williams, Q., Lay, T. & Kellogg, L.H., 1998. Ultralow velocity zones at the core–mantle boundary, in *The Core Mantle Boundary Region, Geodynamic Series*, 28, pp. 97–118, eds Gurnis, M., Wyssession, M., Knittle E. & Buffett, B.A., American Geophysical Union, Washington, DC.
- Grand, S.P., van der Hilst, R.D. & Widiyantoro, S., 1997. Global seismic tomography: A snapshot of convection in the Earth, *GSA today*, **7**, 1–7.
- Houard, S. & Nataf, H.-C., 1993. Laterally varying reflector at the top of D'' beneath northern Siberia, *Geophys. J. Int.*, **115**, 168–182.
- Karason, H. & van der Hilst, R., 2000. Improving global tomography models of P-wavespeed I: incorporation of differential times for refracted and diffracted core phases (PKP, Pdiff), *J. geophys. Res.*, submitted.
- Karato, S.I., 1998. Some remarks on the origin of seismic anisotropy in the D'' layer, *Earth Planets Space*, **50**, 1019–1028.
- Kendall, J.-M. & Shearer, P.M., 1994. Lateral variations in D'' thickness from long period shear wave data, *J. geophys. Res.*, **99**, 11 575–11 590.
- Kendall, J.-M. & Silver, P.G., 1996. Constraints from seismic anisotropy on the nature of the lowermost mantle, *Nature*, **381**, 409–412.
- Kendall, J.-M. & Silver, P.G., 1998. Investigating causes of D'' anisotropy, in *The Core Mantle Boundary region, Geodynamic Series*, 28, pp. 97–118, eds Gurnis, M., Wyssession, M., Knittle, E. & Buffett, B.A., American Geophysical Union, Washington DC.
- Kennett, B.N.L., Engdahl, E.R. & Buland, R., 1995. Constraints on seismic velocities in the Earth from traveltimes, *Geophys. J. Int.*, **122**, 108–124.
- Lay, T. & Helmberger, D.V., 1983. A lower mantle S-wave triplication and the shear velocity structure of D'' , *Geophys. J. R. astr. Soc.*, **75**, 799–837.
- Lay, T., Williams, Q., Garnero, E.J., Kellogg, L. & Wyssession, M.E., 1998. Seismic wave anisotropy in the D'' region and its implications, in *The Core Mantle Boundary Region, Geodynamic Series*, 28, pp. 299–318, eds Gurnis, M., Wyssession, M., Knittle, E. & Buffett, B.A., American Geophysical Union, Washington DC.
- Lithgow-Bertelloni, C. & Richards, M.A., 1998. The dynamics of Cenozoic and Mesozoic plate motions, *Rev. Geophys.*, **36**, 27–78.
- Matzel, E., Sen, M.K. & Grand, S.P., 1996. Evidence for anisotropy in the deep mantle beneath Alaska, *Geophys. Res. Lett.*, **23**, 2417–2420.
- Maupin, V., 1994. On the possibility of anisotropy in the D'' layer as inferred from the polarization of diffracted S-waves, *Phys. Earth planet. Inter.*, **87**, 1–32.
- Müller, G., 1985. The reflectivity method: a tutorial, *J. Geophys.*, **58**, 153–174.
- Pulliam, J. & Sen, M.K., 1998. Seismic anisotropy in the core–mantle transition zone, *Geophys. J. Int.*, **135**, 113–128.
- Ritsma, J., van Heijst, H.J. & Woodhouse, J.H., 1999. Complex shear wave velocity structure imaged beneath Africa and Iceland, *Science*, **286**, 1925–1928.
- Russell, S.A., Lay, T. & Garnero, E.J., 1999. Small-scale lateral shear velocity and anisotropy heterogeneity near the core–mantle boundary beneath the central Pacific imaged using broadband ScS-waves, *J. geophys. Res.*, **104**, 13 183–13 199.
- Scherbaum, F., Krüger, F. & Weber, M., 1997. Double beam imaging: mapping lower mantle heterogeneities using combinations of source and receiver arrays, *J. geophys. Res.*, **102**, 507–522.
- Silver, P.G. & Chan, W.W., 1991. Shear-wave splitting and subcontinental mantle deformation, *J. geophys. Res.*, **96**, 16 429–16 454.

- Thomas, Ch. & Weber, M., 1997. P velocity heterogeneity in the lower mantle determined with the German Regional Seismic Network: improvements of previous models and results of 2D modelling, *Phys. Earth planet. Inter.*, **101**, 105–117.
- Thomas, Ch., Weber, M., Wicks, C. & Scherbaum, F., 1999. Small scatterers in the lower mantle observed at German broadband arrays, *J. geophys. Res.*, **104**, 15 073–15 088.
- Thomas, Ch., Kendall, M. & Weber, M., 2002. Images of D'' beneath northern Asia: (1) Multi-azimuth studies of heterogeneity, *Geophys. J. Int.*, **151**, this issue.
- Vidale, J.E. & Hedlin, M.A.H., 1998. Evidence for partial melt at the core mantle boundary north of Tonga from the strong scattering of seismic waves, *Nature*, **391**, 682–685.
- Vinnik, L., Farra, F. & Romanowicz, B., 1989. Observational evidence for diffracted SV in the shadow of the Earth's core, *Geophys. Res. Lett.*, **16**, 519–522.
- Vinnik, L., Romanowicz, B., LeStunff, Y. & Makeyeva, L., 1995. Seismic anisotropy in the D'' layer, *Geophys. Res. Lett.*, **22**, 1657–1660.
- Weber, M., 1993. P- and S-wave reflections from anomalies in the lowermost mantle, *Geophys. J. Int.*, **115**, 183–210.
- Weber, M. & Davis, J.P., 1990. Evidence of a laterally variable lower mantle structure from P- and S-waves, *Geophys. J. Int.*, **102**, 231–255.
- Wen, L. & Helmberger, D.V., 1998. Ultra low velocity zones near the core-mantle boundary from broadband PKP precursors, *Science*, **279**, 1701–1703.
- Wessel, P. & Smith, W.H.F., 1991. Free software helps map and display data, *EOS, Trans. Am. geophys. Un.*, **72**, 441, 445–446.